Experimental and Numerical Analysis of Titanium/HA FGM for Dental Implantation

S. Sazesh & A. Ghassemi*
Department of Mechanical Engineering,
Najafabad Branch, Islamic Azad University, Najafabad, Iran
E-mail: sinasazesh@smc.iaun.ac.ir, a_ghassemi@pmc.iaun.ac.ir
*Corresponding author

R. Ebrahimi
Advanced Materials Research Center,
Department of Materials Engineering,
Najafabad Branch, Islamic Azad University, Najafabad, Iran
E-mail: rezaebrahimi@iaun.ac.ir

M. Khodaei
Center for Advanced Engineering Research,
Majlesi Branch, Islamic Azad University, Isfahan, Iran
E-mail: khodai1358@gmail.com

Abstract: FGM dental implants are a very good alternative with respect to homogenous implants. In this study by focusing on mechanical property as one of the most important factors in implant design, the static behaviour of Ti/Nanostructure HA (hydroxyapatite) FGM dental implant has been fabricated and investigated experimentally and numerically. At the first step, the nanostructure hydroxyapatite powders were synthesized by natural origin. At the second step, the initial powders were cold compacted in order to fabricate Ti/HA FGM samples for 4 different volume fraction exponents (N=1/3, 2/3, 1, 2). Then the compacted powders have been sintered using a vacuum furnace, in which compressive strength of each particular sample was finally assessed. A three-dimensional geometrical model of FGM dental implant system and surrounding bone was created by using the macro programming language in ANSYS software and then finite element analysis under static forces was performed. Finally the experimental results strength tests were compared with numerical solutions. According to the results, the FGM dental implants made of Ti/HA under static forces were sufficiently safe. As a result, FGM sample with volume fraction exponent of N=2/3 was chosen as the best sample.

Biographical notes: S. Sazesh received his MSc in Mechanical Engineering: Manufacturing from University of IAU, Najafabad Branch, Isfahan, Iran in 2016. **A. Ghassemi** is an assistant professor in Mechanical Engineering at IAU, Najafabad Branch. **R. Ebrahimi** is an associate professor in Materials Engineering at IAU, Najafabad Branch. **M. Khodaei** received his PhD in Biomaterials at Isfahan University of Technology in 2015. His research interests are metallic and ceramic biomaterials and nano-bio-composites.

1   INTRODUCTION

Usually, single phase materials with a bioactive coating layer are being used for dental implants. coated metallic implants make stress shielding in the surrounding bone and over time poor survival of coatings are the current problems resulting severe biocompatibility issues [1]. The problems mentioned above can better be solved by introducing the concept of a functionally graded material (FGM). The gradual distribution of components in an FGM can eliminate the macroscopic interface, such as that in a direct joint of two materials [2].

A typical FGM is an inhomogeneous composite made from different phases of material constituents (usually ceramic and metal). Within FGMs the different microstructural phases have different functions [3]. The required function of a dental implant varies at the outside of the jawbone, inside it, and at jawbone boundary as well [4].

On the outside of the bone, the implant material needs to have sufficient mechanical strength to bear the occlusal force, whereas the part of the jawbone must have stress relaxation, osteoconductivity, and adequate bone-implant bonding strength so that the new bone is created speedily and attaches directly to it. Then we should choose some type of biomaterials to include biometals and bioceramics for FGM dental implants to satisfy these necessary properties simultaneously.

In the last few years, a variety of metallic biomaterials and bioceramics were investigated for FGM dental implants such as titanium/hydroxyapatite (Ti/HA) [2], [5-14], titanium/cobalt (Ti/Co) [5], titanium/zirconia (Ti/ZrO$_2$) [15-17], titanium/silica (Ti/SiO$_2$) [18], titanium nitride/hydroxyapatite (TiN/HA) [19], [20], hydroxyapatite/ partially stabilized zirconia (HA/PSZ) [21], and hydroxyapatite/yttria stabilized tetragonal zirconia (HA/Y-TZP)[22].

Hydroxyapatite (HA, Ca$_{10}$ (PO$_4$)$_6$ (OH)$_2$) is the main mineral constituent of human teeth and bones. It shows excellent biocompatibility with hard tissues and also skin and muscle tissues. Moreover, HA does not exhibit any toxic effects and can directly bond to the surrounding bone. Besides that, HA has mechanical properties close to the human bone[23], [24]. HA is the most well-known biocompatible material for implantation inside the bone [25]. There are several methods for the fabrication of FGM and porous FGM dental implants such as cold isostatic pressing (CIP) [7], [15], [18], spark plasma sintering (SPS) [8], [10], [11], [19], [22], hot pressing [6], [12], [13], [16], [21], and powder metallurgy (PM) [2], [5], [8], [9], [14], [17], [26-30].

The powder metallurgy (PM) process is a suitable route for FGM fabrication [31]. In the PM process, the waste metal is significantly less than other methods. From economical aspect, this method is affordable and available [32].

A combination of biological and biomechanical factors is responsible for the failure of supported fixed prostheses. Contrary to natural teeth, the biologic aspects of implants problems are fairly low. The most common problems of implants which have a biomechanical origin occurs after loading on implant [33].

Many studies of the biomechanical responses of conventional dental implants have been reported [34-41]. Despite their clinical importance, research concerning the static and dynamic characteristics of FGM implants is still limited.

Without considering the effect of surrounding trabecular bone, Hedia and Mahmoud employed a two-dimensional axisymmetric finite element model to investigate the stress distribution in an FGM implant subjected to an axial static load [42]. Hedia later improved the analysis by including this effect in another numerical investigation [43]. It should be noted that the configurations of tooth and jaw are neither planar nor symmetric, but are highly irregular.

In addition, inclined occlusal forces may often be applied, which makes the implant/bone system neither in a plane state nor in a symmetric state. Hence, it is important that a three-dimensional model, incorporating the interaction between the implant and the surrounding bone, be adopted to provide a more accurate interpretation of the stress and displacement distributions in the implant and the peri-implanted bone tissues.

In a comprehensive parametric study, Yang and Xiang studied the biomechanical behavior of an FGM dental implant in surrounding bone by using a three-dimensional finite element method (FEM) [44]. They highlighted the influence of the material properties, the volume fraction index, the occlusal force orientation, and the osseointegration quality on the maximum von-Mises stress, deformation distribution, natural frequencies, and harmonic response. They reported a larger volume fraction index that helps to reduce the maximum stress difference at the implant–bone interfaces and slightly raises the fundamental frequency, but significantly increases the amplitudes of maximum stresses and displacements under dynamic forces.

Lin et al., evaluated bone remodeling when replacing the titanium dental implant with a hydroxyapatite/ collagen (HAP/Col) FGM model. At their study, the remodeling simulation was performed over a 4 year healing period. They reported that FGM dental implant can better stimulate bone remodeling activity, and relieve the peak stress in the cancellous peri-implant tissues, however; more HAP/Col content in FGM can causes the reduction in structural stiffness [45].

Another study by Lin et al. explores an optimal design of FGM dental implant for promoting a long-term success by using the computational bone remodeling and design optimization. They reported a better performance in bone turnover which can be achieved by lowering the FGM material gradient, but this will at the same time reduce the stiffness of implantation, consequently placing the bone–implant interface at higher risk of damage during the early healing stage. According to their research, this problem can be solved by the multi-objective optimization processes, which are yet to be employed in biomechanical studies up to date [46].

Despite the ability of finite element software for processing data, one of the greatest challenges to analysis dental implants are difficulties to modeling human maxilla and mandible, simulation mechanical behavior of implants and the force applied on them. Material properties and boundary conditions at dentistry are very complicated and often there is no information about it, so a set of assumptions at finite element analysis are applied and stress-strain response models are rebuild simpler.

Applying these assumptions in addition to facilitating modeling also affected the accuracy of results [47]. Because of these simplifications at finite element analysis, it is important to verify numerical results with experimental tests. In fact, just a finite element analysis without considering the real conditions cannot guarantee the safety of dental implants under static and dynamic loading. At previous studies, there was no comparison between numerical and experimental FGM dental implants strength and no previous work has been done. In this study commercially pure Ti (CP-Ti) was chosen as metallic phase of FGM dental implants because of its good mechanical properties (elastic modulus, toughness, fatigue, and strength), excellent corrosion resistance compared with other metallic biomaterials, good biocompatibility, high strength per weight ratios, benign and safe biologic response, low density, resistance against electrochemical decomposition and destruction [23], [24], [48]. However Ti and its alloys have sufficient mechanical properties but they are bioinert and cannot promote tissue bonding to the implants. To improve bioactivity of dental implants and increase Osseointegration, HA was chosen as a bioceramic phase for FGM samples.

The main objective of this paper is to fabricate a FGM dental implant with suitable mechanical properties by focusing on strength and good biocompatibility to eliminate exciting problems of currently coated implants.

To reach these purposes at the first step, Ti/HA FGM dental implants has been fabricated by powder metallurgy technique at different volume fraction exponents and strength of samples has been investigated using compression tests at two parts including richer Ti region and richer HA region. At the second step three-dimensional finite element method were applied to compare results of experimental tests with FEM results under static loading. Extensive numerical results are obtained to show the influences of material properties and compositional profile on the static behavior of the FGM dental implant and surrounding bone system.

2 EXPERIMENTAL PROCEDURE

2.1. Raw materials and powder processing

To fabricate FGM implants, the powder metallurgy method was applied. As compositions of FGMs, titanium and hydroxyapatite powders were chosen. Commercially pure titanium (CP-Ti) grade 4 with a particle size smaller than 44 micrometers (325 meshes) and irregular morphology (Baoji Unique Titanium Industry Co. LTD- China) were used as the metallic phase. The chemical composition of Ti powder was (Wt.%): Ti>99.5, O<0.4, Fe<0.07, C<0.02, H<0.02, N<0.02.

Hydroxyapatite was derived from bovine bone according to following steps:

(1) Diaphysis part of bovine femoral bone was boiled for 2h and the bone marrow and all pieces of meat and fat were removed.

(2) By applying direct flame to the cleaned bone for 2h at the temperature of 400 °C, organic components (collagen) were burned. The product of this thermal process contained some char due to burning of organic components.

(3) To remove the remaining char, the black powder (bone ash) was placed in an air furnace at the temperature of 800 °C for 2h and finally, it was cooled inside the furnace. Bahrololoom et al., showed that the best heat treatment temperature for the conversion of bone ash to hydroxyapatite was 800 °C. The optimum temperature for heat treatment was found to be 800 °C.

(4) The particle size of the heat treated bone ash was milled for 16:30′h to get a fine powder. A planetary ball mill system consisting of an alumina cup and balls was used to prepare fine particles after heat treating.

The feed ratio was 18.5 g powder to 96 g ball (1 to 5 weight ratio). The speed was fixed at 250 rpm and the milling time was set at 16:30′h with pause and reverse mode (Fig. 1).

Fig. 1   Hydroxyapatite powder after heating in air furnace

2.2. Powder pressing mold

Mixture of Ti and HA powders were cold compacted using a biaxial cylindrical mold (H= 20 mm, D= 6 mm) to obtain better uniformity of mechanical properties (Fig. 2).
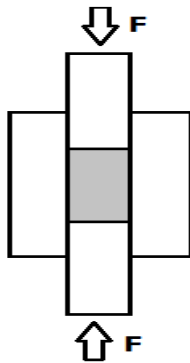

Fig. 2   Symbolic design of biaxial powder presses mold

2.3. Fabrication of Ti/HA FGM

To fabricate Ti/HA FGMs with different volume fractions, weight values of Ti and HA powders for each layer were calculated and were mixed with 2 wt.% aqueous solution- %5 polyvinyl alcohol (PVA), then they were pressed biaxial layer by layer (every layer with different ratio of Ti/HA) adjusted to pre-designed compositional profile of Ti/HA FGM into the cylindrical mold at the pressure of 250 MPa by universal apparatus (HOUNSFIELD, H50KS) at the ambient temperature.

2.4. Ti and HA powder weight values calculation

Titanium and hydroxyapatite powders weight values for each layer were calculated using a simple rule of

mixture of composite materials (Voigt model) and MATLAB software (R2009a) was utilized. The titanium volume fraction can be represented as following function of the distance along the Z axis, Eq. (1).

$$V_{Ti} = \left(\frac{2Z+h}{2h}\right)^N \tag{1}$$

Where h is the thickness of the structure, and N ($0 \leq N \leq \infty$) is a volume fraction exponent, which dictates the material variation profile through the FGM layer thickness. In this study, four different volume fractions (N= 1/3, 2/3, 1 and 2) were considered to compare the effects of volume fraction changes on mechanical properties. Coordinate of Z ($-h/2 \leq Z \leq h/2$) function is chosen at the center of FGMs as shown in Fig. 3. The volume fraction of HA is:

$$V_{HA} = 1 - V_{Ti} \tag{2}$$

The effective material properties P_f of the FGM layer, like Young's modulus E_f, and thermal expansion coefficient α_f, can then be expressed as:

$$P = P_m V_m + P_c V_c \tag{3}$$

Where P_m and V_m are the material properties and volume fraction of the metallic phase (Ti) and P_c and V_c are the material properties and volume fraction of the ceramic phase (HA). Table 1 lists the Young's modulus, Poisson's ratio, and mass density of the materials used in this experimental study.
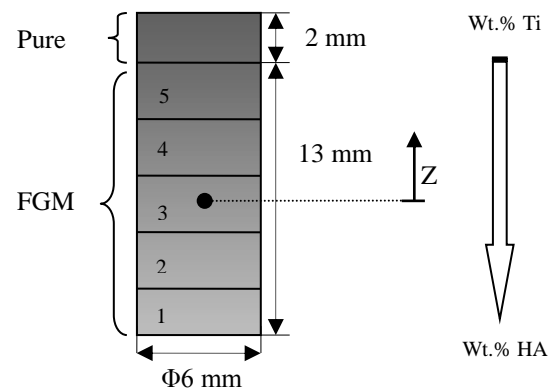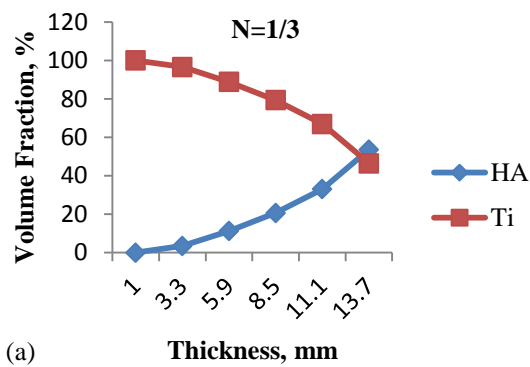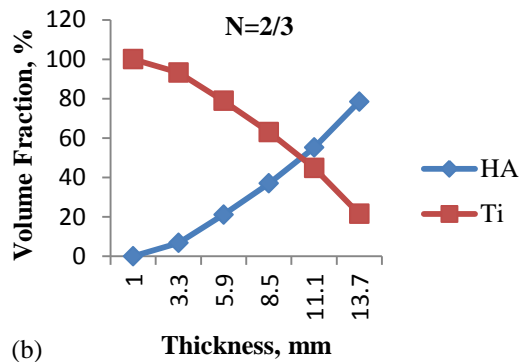

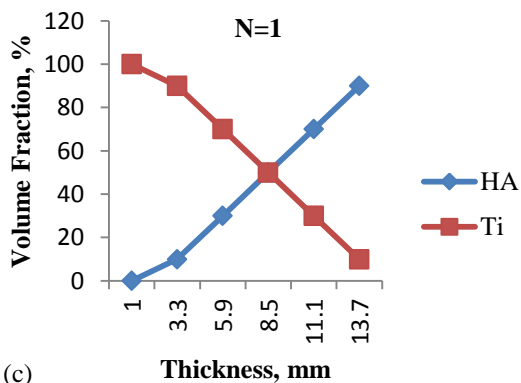**Fig. 3**   Dimensions and configuration of FGM dental implant in the experimental study

Eqs. (1) and (2) give a composition profile changing continuously from Ti-rich at the top end to the HA-rich at the bottom. As shown in Fig. 4, the pre-designed compositional profile of Ti/HA FGMs is affected by different volume fraction exponents.
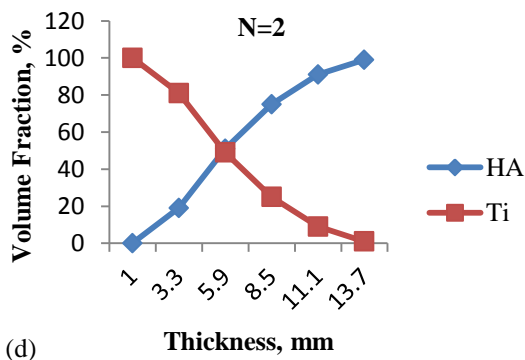
(a)

(b)

(c)

(d)

Fig. 4   Pre-designed compositional profile of Ti/HA FGM at different volume fraction exponents, (a) N=1/3; (b) N=2/3; (c) N=1; (d) N=2

2.5. FGM samples sintering

A thermal cycle to remove glue and also to sinter the pellets was chosen based on Fig. 5. This thermal cycle was carried out in a vacuum furnace with a vacuum level of 1×10^{-4} Torr. At first, samples were heated at 200 °C and to eliminate humidity, they were kept at this temperature for 1 h. After that, samples were heated up to 500°C and kept at this temperature for 1 h to eliminate glue, then up to 800 °C were heated for 2 h kept at this temperature and were heated up to 1100 °C and kept at this temperature for 2 h to complete two steps sintering process [49]. All heating steps were performed at the rate of 5 °C/min.
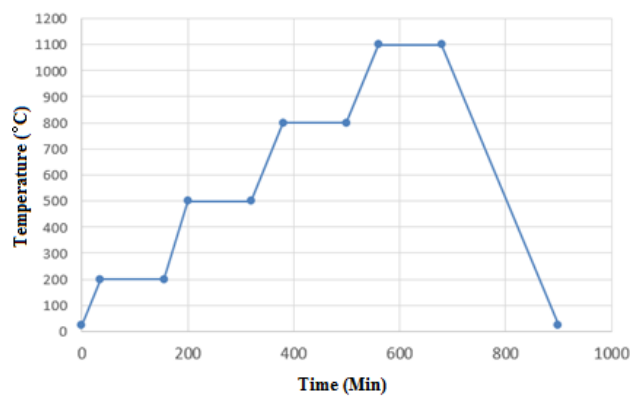

Fig. 5   The thermal cycle which was used for sintering of Ti/HA FGM [51].

2.6. Mechanical properties evaluation

To investigate the strength of FGM samples, compression tests were used with a crosshead speed of 1 mm/min. After sintering process, the length of samples increased to 18 mm due to porosity. So to investigate the strength of Ti/HA FGMs at different critical regions, the samples were cut by saw to 2 parts including Ti riched region and HA riched region. Compression tests applied by a universal testing machine (HOUNSFIELD: H30KS: UK) device and engineering stress-strain diagrams were drawn and required data was extracted.

3   NUMERICAL STUDY

3.1. FGM dental implant modeling

A 3-D model of a mandibular section of bone with missing second premolar and its superstructures were used in this study. For simulation, a commercially type dental implant (Nobel Biocare, Branemark, Gothenburg, Sweden) was used. As threads can maximize the contact surface area and improve implant stability[50, 51], a V-threaded FGM implant with an

interval of 1.2 mm and an angle of 60° was used in this study[44, 52]. The implant (15 mm in height and 3.7 mm in diameter) and the 7 mm long Ti abutment were connected by an internal screw (13 mm in height and 1 mm in diameter). The implant–abutment structure was implanted in the mandibular section where the trabecular bone is surrounded by a 2 mm thick cortical bone layer (Fig. 6). The mesial and distal section planes were not covered by cortical bone.
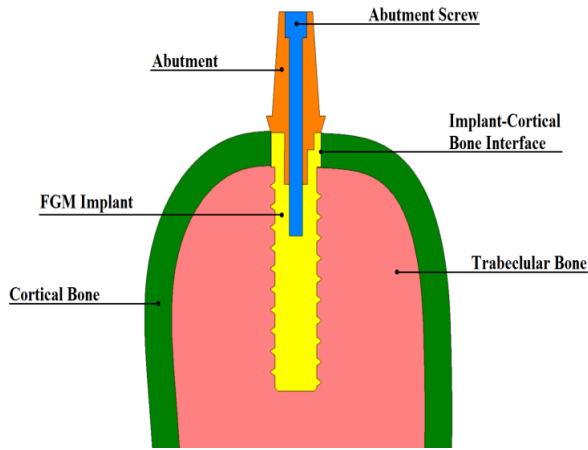

Fig. 6   A section of FGM dental implant/bone system

The three-dimensional geometrical model of the implant/surrounding bone system was created using the CAD/CAM software (CATIA V5R19). The geometry of the human mandible takes the shape of that created from a CT database through image segmentation and spline reconstruction[35]. At first, every single part of the dental implant system and surrounding bone including fixture, abutment, screw, cortical bone and trabecular bone were modeled in CATIA software. Models from Part Design and Assembly Design workbenches of CATIA software were transferred to drafting workbench. Then detail and assembly drawing have been prepared along with a complete detail of shapes and dimensions as a design for manufacturing (DFM). In Fig. 7 draft of the fixture has been shown as the main part of this study.
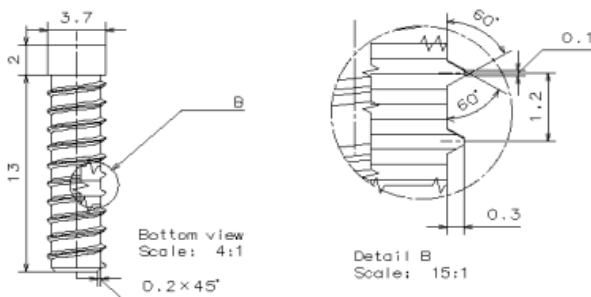

Fig. 7   Configuration of the FGM implant and details of the thread

For numerical solution, finite element method (FEM) was used to analysis model by ANSYS 14, Mechanical APDL. To ensure the full and impeccable modeling of components in ANSYS software, the assembled model of FGM dental implant/surrounding bone system in ANSYS finite element software was remodeled by macro programming language.

3.2. Material properties assumption

In this study the abutment, internal screw, cortical bone, and trabecular bone are treated as linear isotropic homogeneous elastic materials. Table 1 lists Young's modulus, Poisson's ratio, and mass density of the materials used in the numerical examples. The fixture component is Ti/HA FGM so phases change gradient and with changing Ti phase to HA phase, gradually along longitudinal direction, the material properties change gradually too.

Table 1. Material properties used in the numerical study

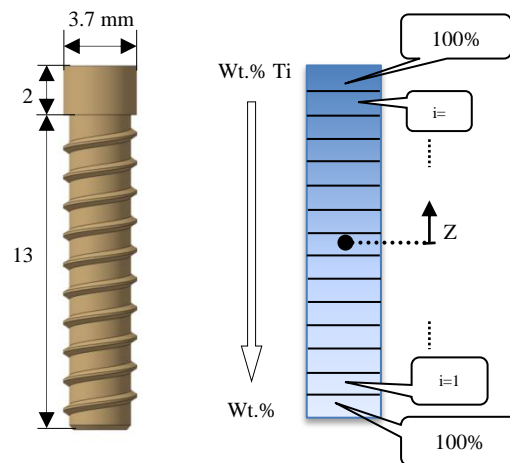| Material	E (GPa)	v	ρ (kg/m^3)	Reference
Abutment	110	0.35	4500	Yang and Xiang[44]
Screw	110	0.35	4500	Yang and Xiang[44]
Cortical Bone	14	0.3	1700	Rho et al.[53]
Trabecular Bone	3	0.3	270	Rho et al.[53]
Ti	110	0.35	4500	Benzing et al.[54] and Lin et al.[38]
HA	40	0.27	3219	Hedia and Mahmoud[42]

Fig. 8   Configuration of the FGM dental implant with layer details

The FGM dental implant model in finite element analysis was divided into 15 segments with the same

height. In this structure, the applied occlusal force is mainly carried by the cortical bone around the upper part of the implant. A much higher volume percentage of Ti in this region and more HA in the lower region is desirable, as it can provide sufficient load-carrying capacity and at the same time minimize the material mismatch between the implant and the surrounding bone tissues (Fig. 8).

As mentioned in the previous section, properties of FGM implant in the longitudinal direction (Z-axis) depend on location and effective value (P_f) of them such as young's modulus E_f, and Poisson's ratio (ν_f) at an arbitrary point of the implant, that can be determined by the rule of mixture. From Eqs. (1) through (3) we have:

$$E_f(Z,T) = (E_{Ti} - E_{HA})V_{Ti} + E_{HA} \qquad (4)$$

$$\nu_f(Z,T) = (\nu_{Ti} - \nu_{HA})V_{Ti} + \nu_{HA} \qquad (5)$$

Where E_{HA} and ν_{HA} are young's modulus and poisson's ratio of hydroxyapatite and E_{Ti} and V_{Ti} are young's modulus and poisson's ratio of titanium respectively. Equations (1) and (2) gives a composition profile changing continuously from Ti rich at the top end to HA rich at the bottom (Fig. 9). According to data from Eqs. (4) and (5), the mechanical properties of Ti/HA FGM dental implant for different volume fraction exponents are presented in Figs. 10 and 11. Mechanical properties of Ti/HA FGMs change gradually from one side to another one. The numbers of layers were determined in Fig. 8. In finite element analysis for FGM samples, 15 layers were used which are pure HA and Ti in the first layer and the last one respectively.
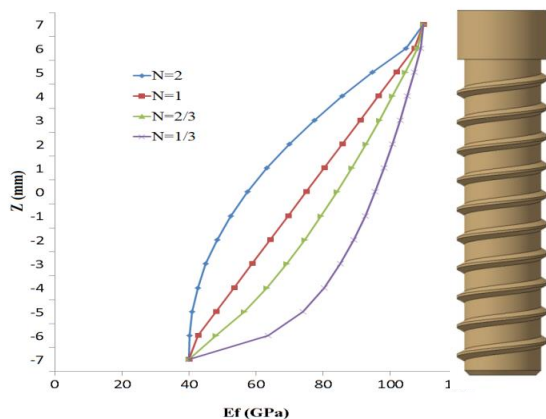

Fig. 9   Longitudinal variation in material properties of FGM implant

As shown in Figs. 10 and 11, with increasing volume fraction of Ti along layers, the young's modulus and

Poisson's ratio increases gradually but the gradient of diagrams varies with different volume fraction exponents (N).
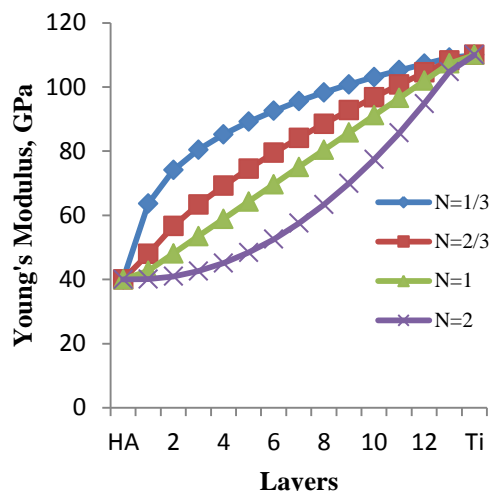

Fig. 10   Relationship between young's modulus and layers in Ti/HA FGM
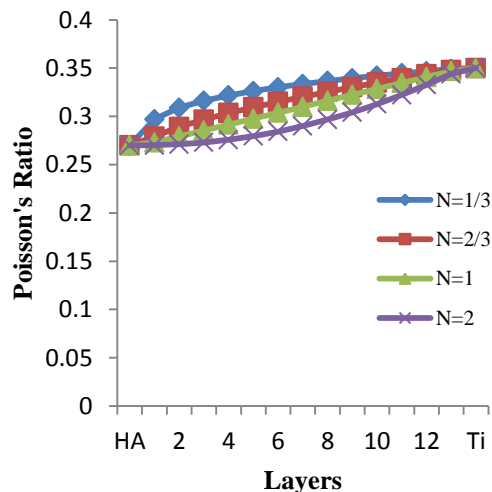

Fig. 11   Relationship between poisson's ratio and layers in Ti/HA FGM

3.3. Interface conditions

To definition interface conditions between implant-bone surfaces, it was assumed that osseointegration was established completely (100%) which does not necessarily simulate clinical situations. These are inherent limitations of this study, so in software the interface condition was bonded between all surfaces in the fixture-bone interface. The similar interface condition (bonded) was assumed between fixture-abutment, abutment-screw and fixture-screw as well.

The ''bonded'' type simulates perfect osseointegration in which the implant and the surrounding cortical bone are fully integrated so that neither sliding nor separation in the implant–cortical bone interface is possible [44]. In quick loading finite element studies, it has been proved that friction coefficient changes have not significant effects on increase or decrease of compressive or tensile stresses of the bone [47]. So all surfaces of model merge together in ANSYS software and friction contact on jawbone is ignored.

3.4. Finite element modeling

Finite element model required in FE analysis is created by discrediting the geometric (i.e. CAD) model into smaller and simpler elements. Hexahedron elements in the fixture, abutment, screw, cortical bone and trabecular bone correspond to SOLID45 type elements in ANSYS element library with each node having three degrees of freedom. SOLID45 is used for the 3-D modeling of solid structures. The element is defined by eight nodes having three degrees of freedom at each node: translations in the nodal x, y, and z directions (Fig. 12). The element has plasticity, creep, swelling, stress stiffening, large deflection, and large strain capabilities. A reduced integration option with hourglass control is available [55].

The number of elements for FEM model and each component are presented in Table 2 and in the following the finite element models are shown in Fig. 13.
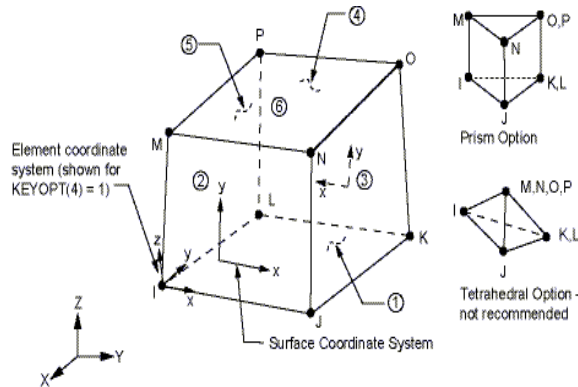

Fig. 12   SOLID45 Geometry [57]

Table 2   Number of elements in FE model

Component	Element
Abutment	974
Screw	871
Fixture	10093
Cortical Bone	2153
Trabecular Bone	12145
Total	26236

3.5. Loading and boundary conditions

Loading of the implants, in 3-D, with forces of 17.1 N, 114.6 N, and 23.4 N in a lingual, an axial, and a mesiodistal direction, respectively (Fig. 14), simulated average masticatory force in a natural, oblique direction. These components represented the masticatory force of 118.2 N in the angle of approximately 75° to the occlusal plane. The force magnitudes, as well as the acting point, were chosen based on the work of Mericske-Stern [56].
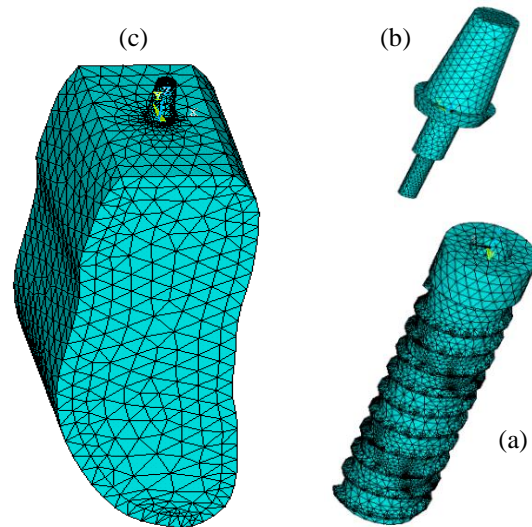

Fig. 13   Finite element meshes view of (a) fixture, (b) abutment and screw and (c) the integrated system
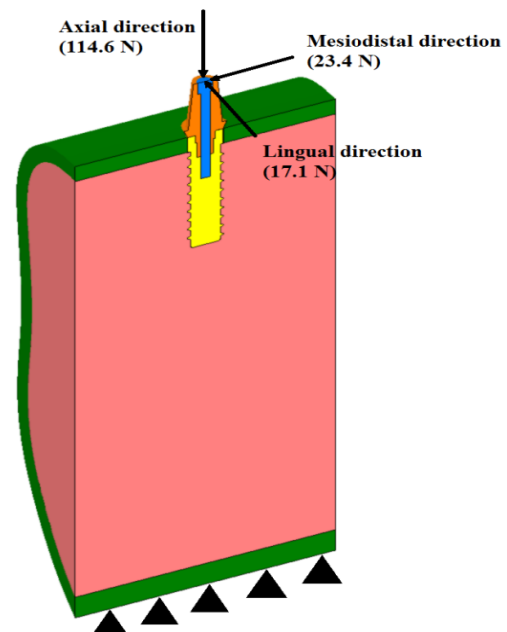

Fig. 14   Applied loads and boundary conditions in FEM model

The FEM model was fixed at the bottom surface of mandibular as shown in Fig. 14 and models were constrained in all directions at the nodes on the mesial and distal bone too. The dental implant/supporting bone system shown in Fig. 14 comprises a Ti/HA implant, a metallic abutment, an internal screw connecting the implant and abutment, and surrounding trabecular bone and cortical bone in the mandibular section. The occlusal force is exerted directly on the top of the abutment and then transmitted down to the implant through the screw connection from its upper part to the middle and lower parts implanted in the trabecular bone.

4   EXPERIMENTAL RESULTS AND DISCUSSION

In the following, the average stress-strain diagrams for every Ti/HA FGM samples in Figs. 15-22 are presented and then the average compressive yield strength (σ_{yc}) and average strain at the σ_{yc} point for FGM samples with different volume fraction exponents are shown in Table 3.

$\sigma yc = 13.634$ MPa
ε in $\sigma yc = 0.051$

Fig. 15   The average engineering stress-strain diagram for FGM implant with N=1/3 at Ti riched region

$\sigma yc = 11.459$ MPa
ε in $\sigma yc = 0.03$

Fig. 16   The average engineering stress-strain diagram for FGM implant with N=1/3 at HA riched region

$\sigma yc = 26.102$ MPa
ε in $\sigma yc = 0.039$

Fig. 17   The average engineering stress-strain diagram for FGM implant with N=2/3 at Ti riched region

$\sigma yc = 5.234$ MPa
ε in $\sigma yc = 0.024$

Fig. 18   The average engineering stress-strain diagram for FGM implant with N=2/3 at HA riched region

$\sigma yc = 14.791$ MPa
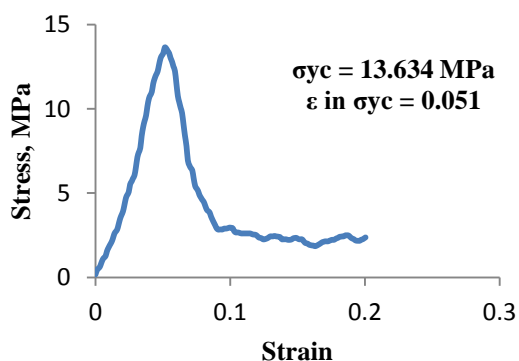ε in $\sigma yc = 0.063$

Fig. 19   The average engineering stress-strain diagram for FGM implant with N=1 at Ti riched region

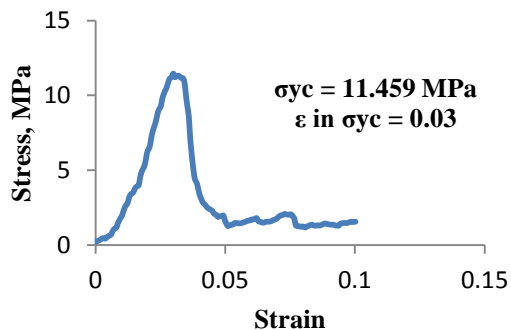**Fig. 20**   The average engineering stress-strain diagram for FGM implant with N=1 at HA riched region
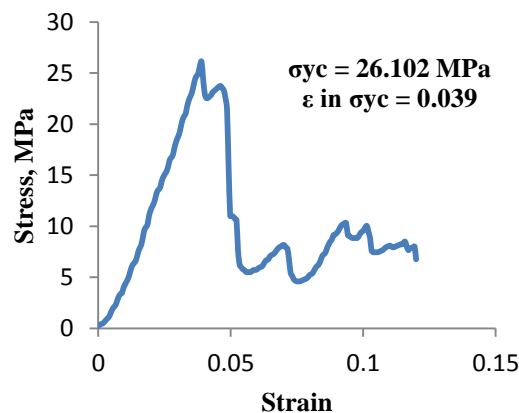

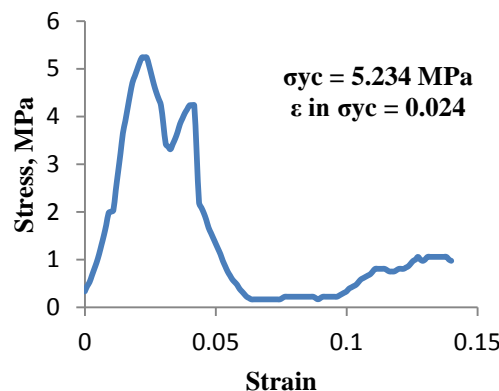**Fig. 21**   The average engineering stress-strain diagram for FGM implant with N=2 at Ti riched region

Fig. 22   The average engineering stress-strain diagram for FGM implant with N=2 at HA riched region
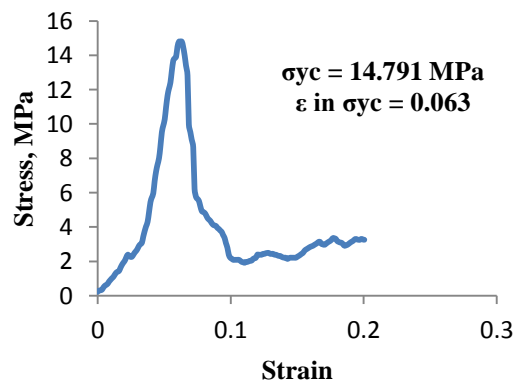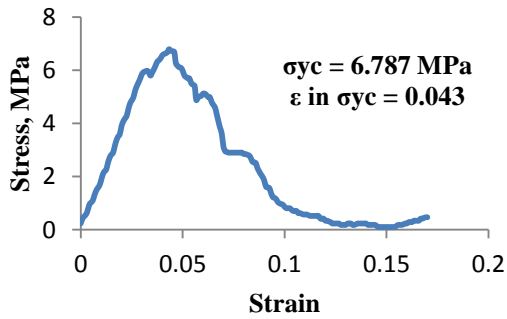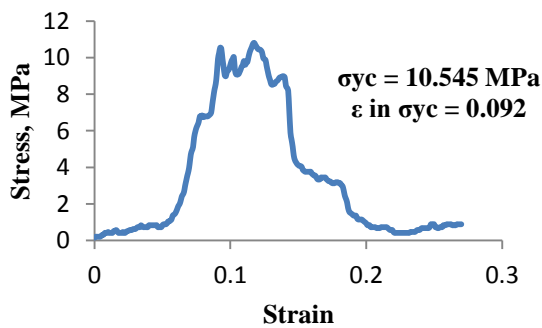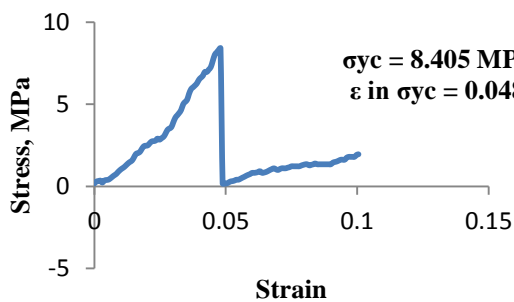
Table 3   The compressive yield strength of FGM implants.

| i | N | σ_{yc}, MPa | | ε in σ_{yc} | |
		Ti region	HA region	Ti region	HA region
1	1/3	13.634	11.459	0.051	0.03
2	2/3	26.102	5.234	0.039	0.024
3	1	14.791	6.787	0.063	0.043
4	2	10.545	8.405	0.092	0.048

Table 4 shows the average displacement of FGM implants with different volume fraction exponents from the compression tests to compare with numerical results.

Table 4   Average displacement of FGM samples at σ_{yc} point.

| i | N | displacement at σ_{yc} , mm | |
		Ti region	HA region
1	1/3	0.459	0.27
2	2/3	0.351	0.216
3	1	0.567	0.387
4	2	0.828	0.432

According to diagrams and results of compression tests in Table 3, the compression yield strength (σ_{yc}) for samples with N=2/3 at Ti riched region is higher than other samples (26.102 MPa). For regions with more HA content the samples with N=1/3 showed better strength(11.459 MPa) because at these type of samples, the Ti content is more than other types and inside all layers except first one, which is placed in trabecular bone, the percentage of Ti volume fraction is higher than HA. Samples with N=1/3 due to lower HA (as a bioactive phase) cannot satisfy osseointegration property and have not good biocompatibility, so in total by considering all properties such as mechanical properties and osseointegration, the samples with N=2/3 seems to be a better choice for FGM dental implants to satisfy all necessary properties at the same time.

About displacement or strain, reverse results versus strength were observed, that mean at this situation the samples with higher and better compression strength have lower displacement or strain. As shown in Tables 3 and 4, the displacement and strain for samples with N=2/3 is lower than other volume fraction exponents at both regions so we can say that the FGM dental implants with N=2/3 have much more desire strain or displacement as predicted in compression strength tests.

5   NUMERICAL RESULTS AND DISCUSSION

The static analysis was performed on FGM dental implant with N=2/3. According to Hooke's law, the volume fraction changes of FGM functions have no effect on stress in the linear static analysis of samples and volume fraction exponent just changes mechanical properties of layers and strain or displacement. Since in finite element model the amount of force is constant as well as cross section area of FGM samples, by

young's modulus changing the stress will be constant and just result of displacement or strain will be affected. Due to these reasons in static finite element analysis to obtain maximum Von Mises stress value, the static analysis for one of volume fraction exponents is enough and it is equal to maximum Von Mises stress value for other samples with different volume fraction exponents. Maximum Von Mises stresses that occurred at the FGM dental implant/surrounding bone system, fixture, abutment, and bone are presented in Table 5.

Table 5 Maximum Von Mises stresses due to static loads (MPa)

Component	Maximum Von Mises Stress, MPa
FGM dental implant/surrounding bone system	50
Fixture	34.2
Abutment	50
Bone	15.6

5.1. FGM dental implant/surrounding bone system
Figure 23 represents stress distribution in the FGM dental implant/surrounding bone system in static loading. It is observed that under static loading conditions, the maximum Von Mises stress occurred at some part of abutment body and the value is 50 MPa. Abutment is made from pure titanium. For the static loading, the maximum stress value within the abutment body was 10.31% of the yield strength. Maximum stress value at the integrated system of static loading conditions was lower than the yield strength (yield stress point for CP-titanium grade 4 that is 485 MPa [48]).

5.2. Fixture
As shown in Fig. 24, the maximum Von Mises stress under static loading for fixture were focused at some part of the first thread (number 12 layer) and implant cervical which is a junction point between fixture and abutment (pure titanium layer). The maximum Von Mises stress value in fixture obtained 34.2 MPa. According to Fig. 8 the last layer is pure Ti and number 12 layer is a mix of Ti and HA but the percentage of pure Ti volume fraction is much more (92.15%). If we assume complete osseointegration by use of Eq. 3 the compressive yield stress of this layer (number 12) is:

$$\sigma_{yc} = \sigma_{ym}V_m + \sigma_{yc}V_c = 453.9925 \ MPa \tag{6}$$

where σ_{yc} is compressive yield strength for number 12 layer, σ_{ym} and σ_{yc} are pure Ti yield strength (485 MPa [48]) and HA compressive yield strength (90-400 MPa [24]) respectively. V_m and V_c are volume fraction of titanium (0.9215) and volume fraction of

hydroxyapatite (0.0785). The maximum Von Mises value in pure Ti layer and number 12 layer were 7.05% and 7.53% of yield strength respectively, so the maximum Von Mises stress value in fixture under static loading for both critical layers did not reach the yield strength.
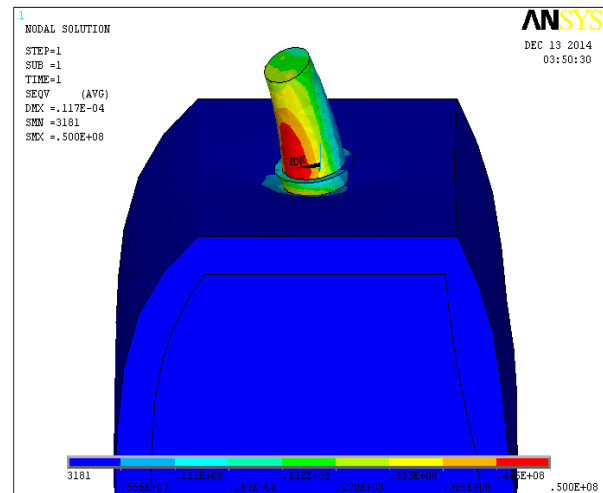

Fig. 23 The Von Mises stress distribution in the FGM dental implant/surrounding bone under static loading
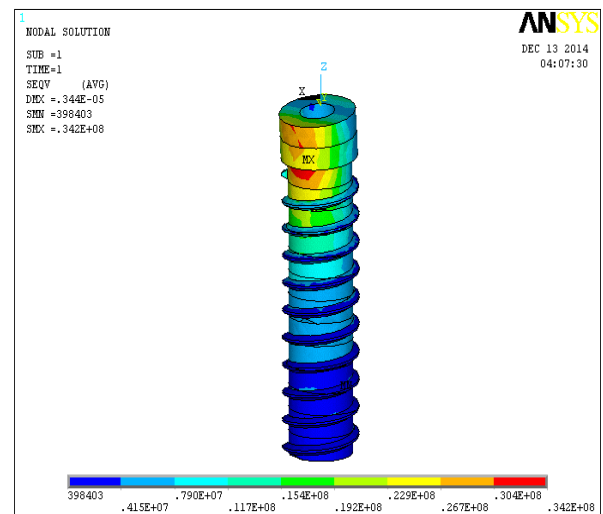

Fig. 24 The Von Mises stress distribution in Ti/HA FGM fixture under static loading

5.3. Abutment
Figure 25 shows stress distribution in abutment under static loading. The maximum Von Mises stress was located at the abutment body. The maximum Von Mises stress for abutment made from pure Ti obtained 50 MPa. This stress value is 10.31% of yield strength, so the maximum Von Mises stress under static loading on abutment body was lower than yield strength (the yield stress point for CP-Ti is 485 MPa).
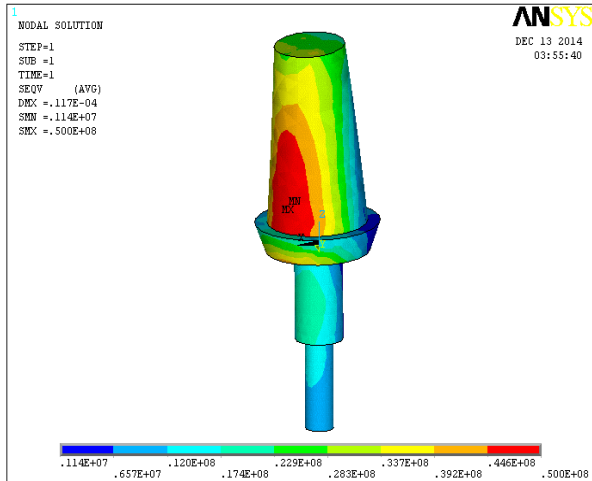
Fig. 25　The Von Mises stress distribution in abutment and screw under static loading

5.4. Cortical and trabecular bone

Maximum stresses were located within the cortical bone surrounding the implant and within the cervical of fixture (Fig. 26). There was no stress within the trabecular bone. Maximum Von Mises stress value within the cortical bone surrounding the implant neck was 15.6 MPa under static loading. For the static loading, the maximum stress value within the cortical bone was 9.18% of the yield stress (compressive yield stress point for cortical bone is 170-193 MPa [24]). For static loading conditions, maximum Von Mises stress value in the cortical bone did not reach the yield strength.
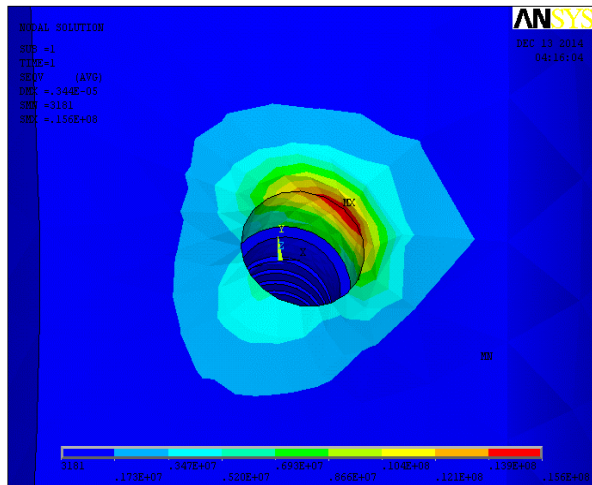

Fig. 26　The Von Mises stress distribution in cortical and trabecular bone under static loading

The locations of critical elements in stress distribution images and results of maximum Von Mises stresses were very close to previous studies [34, 44, 57]. The FEM analysis that was performed at this study

confirmed the safety of Ti/HA FGM dental implants under static loading conditions.

5.5. Displacement of Ti/HA FGM implants under static loading

As mentioned before, the volume fraction exponent changes in FGM implants have not effect on stress contour in static loading but will affect displacement. In Table 6 the maximum displacement of FGM samples with different volume fraction exponent is presented.

Table 6　The Maximum displacement values in FGM implants under static loading.

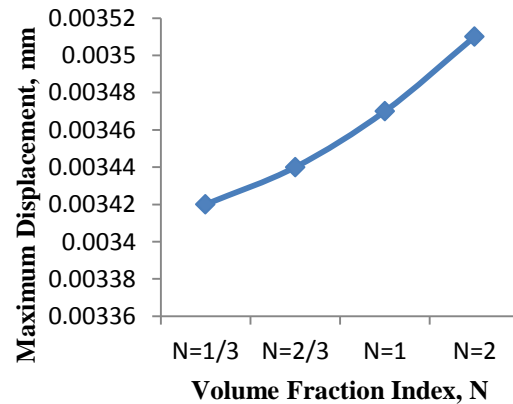| Component	Displacement, mm			
	N=1/3	N=2/3	N=1	N=2
FGM dental implant/surrounding bone system	0.0117	0.0117	0.0117	0.0117
Abutment	0.0117	0.0117	0.0117	0.0117
Fixture	0.00342	0.00344	0.00347	0.00351
Bone	0.00342	0.00344	0.00347	0.00351

Fig. 27　Maximum displacements in FGM fixture with volume fraction exponent changes under static loading

It is observed that in FGM fixture by increasing volume fraction exponent, the displacement value increases due to decreaseing of elastic modulus (Fig. 27). In general, the value of samples displacement under static loading is small. The maximum displacement of the fixture and cortical bone are the same and the value of maximum displacement in an integrated system of FGM dental implant/surrounding bone under static loading occurred in abutment.

The value of displacement in abutment is constant because there is no change in mechanical properties. In Figs. 28-32 the displacement fields for FGM dental implant/surrounding bone system with N=2/3 along with components are shown as a sample.
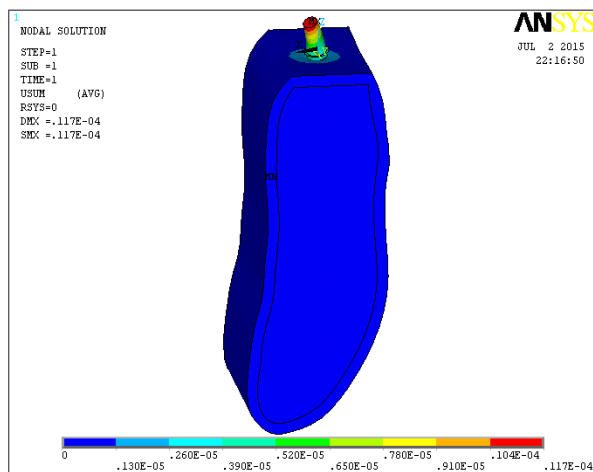
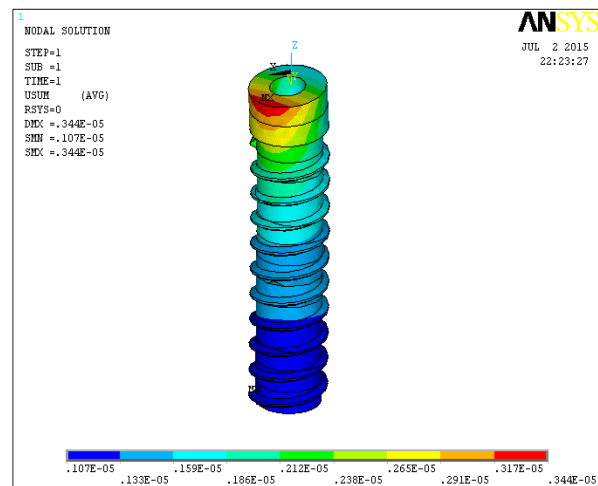**Fig. 28**   The Displacement field for FGM dental implant/surrounding bone system under static loading
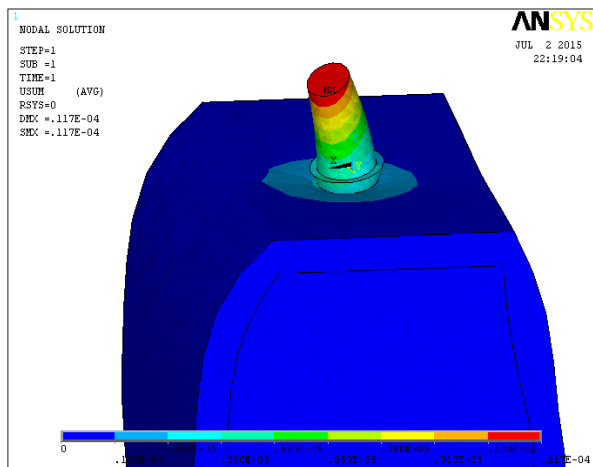

Fig. 29   The Displacement field for FGM dental implant/surrounding bone system under static loading from different view

Fig. 30   The Displacement field for abutment under static loading

Fig. 31   The Displacement field for FGM fixture with N=2/3 under static loading

Fig. 32   The Displacement field for cortical and trabecular bones under static loading

6   COMPARISON ON NUMERICAL AND EXPERIMENTAL RESULTS

To evaluate the precision and accuracy of compression test and to confirm it, the obtained results from experimental tests were compared with the numerical analysis.

6.1. Comparison of the strength results

In compression test every sample is separated to two parts with equal length (9 mm) which includes Ti riched region and HA riched region, so strength comparison was performed for each of two regions with FEM analysis under static loading. The finite element model has 15 distinct layers and separation line of two regions is located in the center of middle layer exactly. While titanium have much more strength

compare with HA bioceramic, so in stress analysis under static loading for FGM implant HA riched region is more critical and sensitive, however, the strength of Ti riched region is important too. In compressive strength tests observed that the failure for both regions occurred in a layer with more HA content.

As shown in Fig. 33, the failure at Ti riched regions has occurred in the middle of layer 3 (Fig. 3) for sintered FGM samples which are equivalent to layer 7 (Fig. 8) from finite element model. For HA riched region, the yield strength occurred in layer number 1 (Fig. 3) for sintered FGM samples which are equivalent to pure HA layer (Fig. 8) from finite element model (Fig. 34). In Fig. 33 the Von Mises stress distribution for FGM dental implant under static loading has been shown to be compared with the strength of sintered FGM samples at Ti riched region.

As shown in Fig. 33, the sintered FGM samples at Ti riched region reach yield strength at specified location during the compression test.
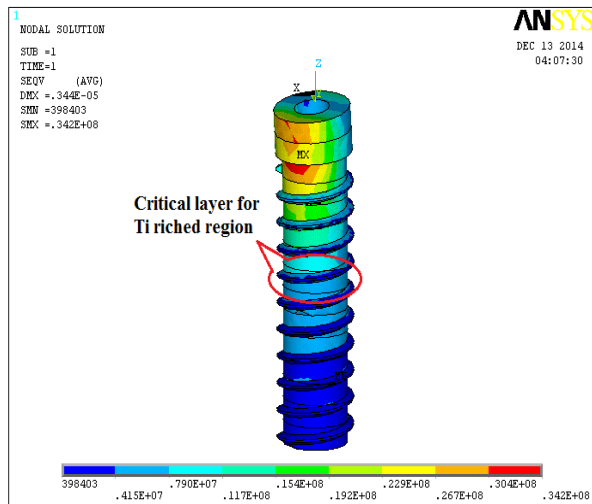
did not reach yield stress. Among of all FGM samples with different volume fraction exponents, the sample with N=2/3 showed the best strength at Ti riched region. In return, the sample with N=2 showed the lowest strength in comparison with other types of FGM samples at Ti riched region. The reason is that the percentage of HA volume fraction in layers of this FGM function (N=2) is more than other types of functions, so it is obvious the yield strength value will be affected by HA content. The more HA content will results in less yield stress.

Fig. 34 shows the Von Mises stress distribution in FGM dental implant under static loading to compare with the strength of sintered FGM samples for HA riched region. In compression test for HA riched region, failure of sintered FGM samples under static loading occurred in specified location as shown in Fig. 34. Because the percentage of HA volume fraction at this region is higher than other layers, in the other words this layer at the FGM samples is more critical.

Fig. 33 The Von Mises stress distribution in Ti/HA FGM implant; the critical layer in compressive strength test specified for Ti riched region
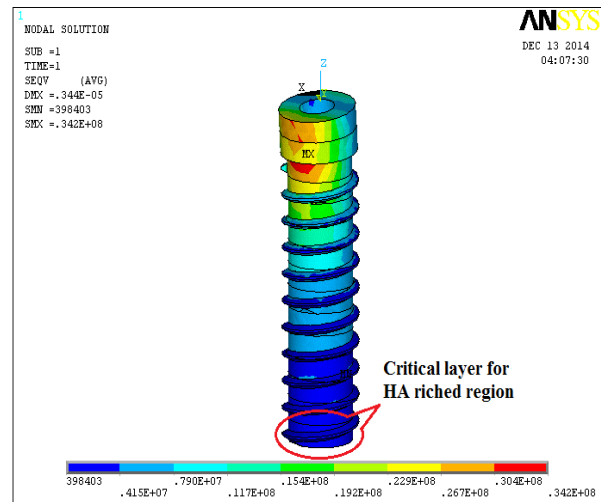
Fig. 34 The Von Mises stress distribution in Ti/HA FGM implant; the critical layer in compressive strength test specified for HA riched region

In this region according to Von Mises stress distribution in numerical solution, the maximum stress under static loading is in the range of 4.15-7.9 MPa while in results obtained from compression test (Table 3), yield stress of Ti riched region for each of volume fraction exponents is higher than maximum stress occurred in finite element model under static loading in critical situation. In compression test the values of yield stresses for volume fraction exponents (N=1/3, 2/3, 1 and 2) for Ti riched region obtained 13.636, 26.102, 14.791 and 10.545 MPa respectively that are higher than maximum Von Mises stress value in FEM analysis. So the strength of Ti/HA FGM dental implants fabricated by powder metallurgy method under static loading for Ti riched region are safe and

Based on the results of the FEM analysis, the maximum Von Mises stress value in the critical layer for HA riched region is in the range of 0.398-4.15 MPa. By comparison between results of FEM analysis with results of experimental tests as presented in Table 3, the maximum Von Mises stress values in critical layer did not reach yield stress in the compression test.

Yield strength values for HA riched region at the experimental test for different volume fraction exponents (N=1/3, 2/3, 1 and 2) are equal to 11.459, 5.234, 6.787 and 8.405 MPa respectively. So the HA riched region under static loading is safe enough and never reach yield strength. It is observed that between different volume fraction exponents, the FGM sample with N=1/3 has the highest strength for HA riched

region due to the low percentage of HA volume fraction in a critical layer in comparison with other exponents at FGM function.

6.2. Comparison of displacement

By comparing displacement results of experimental tests in Table 4 with results of FEM analysis in Table 6, it is observed that the maximum displacement value in FGM fixture under static loading in finite element model is much lower than displacement values in yield point for FGM implants at experimental tests. The displacements in yield point for volume fraction exponents such as 1/3, 2/3 1 and 2 were obtained for Ti riched region 0.459, 0.351, 0.567 and 0.828 mm and for HA riched region 0.27, 0.216, 0.387 and 0.432 mm respectively. As a sample displacement field for FGM dental implant with N=1/3 is shown in Fig. 35. Displacement field in FGM sample with N=1/3 is in the range of 0.0011-0.00342 mm (Fig. 35), while the displacement value in yield stress point at compression test for this sample at Ti riched region was obtained 0.459 mm and at HA riched region was obtained 0.27 mm which are much higher than displacement values under static loading in FEM model for both regions. As a result according to Tables 4 and 5, the strain and displacement values at the yield strength point for FGM implant with N=2/3 had the lowest value among other volume fraction exponents which is an advantage here and indicant more strength of this sample in comparison with other samples of this study.
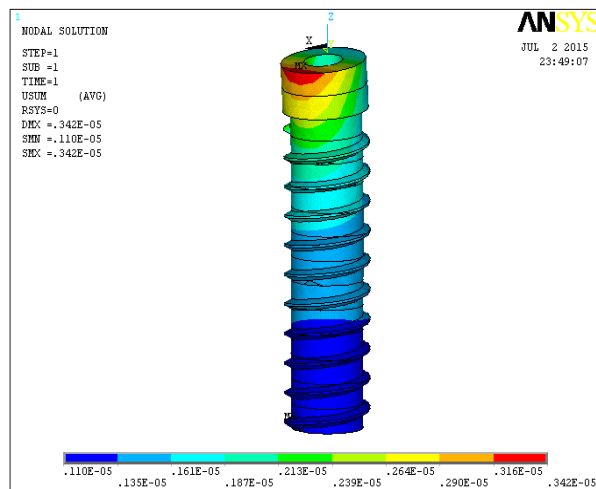

Fig. 35   The Displacement field for FGM fixture with N=1/3 under static loading

According to a comparison between strength and displacement results in experimental tests and numerical solution, the FGM sample with N=2/3 was chosen as the best sample; because not only have optimum strength at richer in Ti and HA regions also can provide suitable bioactivity for osseointegration at lower layers by having sufficient volume fraction of HA. In addition at the yield strength point, it shows less strain.

7   CONCLUSION

One of the most important factors in implant design is the strength of dental implants. So investigation of the static behaviors of dental implants has a vital role in preventing any permanent damage caused by miss-implementation of the implant. But just a FEM analysis cannot guarantee the strength of dental implants at real environment because of some simplifications during analysis; in this study the strength of Ti/HA FGM dental implant fabricated by powder metallurgy method was investigated by FEM analysis and experimental tests which were not found in previous studies. The major conclusions that can be drawn from this study are:

1- The Ti/HA FGM dental implants have been successfully fabricated in four different volume fraction exponents (N=1/3, 2/3, 1, 2) by the powder metallurgy process and sintered in a vacuum furnace with a vacuum level of 1×10^{-4} Torr according to two steps sintering process.

2- Strength of Ti/HA FGM dental implants was investigated by compressive strength test. The average engineering stress-strain diagrams for each sample were drawn and then yield strength and displacement/strain at yield strength point were obtained for Ti riched region as well as HA riched region. The FGM dental implant with N=2/3 had maximum strength among other types of volume fraction exponents at this study and at the same time showed minimum strain value at the yield strength point.

3- Pre-designed compositional profile of Ti/HA FGMs at different volume fraction exponents and mechanical properties of FGM samples in the longitudinal direction by layers has been drawn and gradient changes of properties were evaluated.

4- The static finite element analysis was performed on Ti/HA FGM dental implant and stress distribution for each component under static loading was obtained. According to results, it is observed that the maximum Von Mises stress for every component of FGM dental implant/surrounding bone system was fewer than yield stress; so the safety of Ti/HA FGM dental implants under static loading was confirmed.

5- The displacement field of FGM samples under static loading was obtained and maximum displacement for every component was calculated. It is observed that in

FGM fixture by an increase of volume fraction exponent, the displacement value increases nonlinearly due to a decrease of elastic modulus.

6- By comparison of experimental and numerical results it is observed that yield strength of FGM samples for Ti riched and HA riched regions were more than maximum Von Mises stress under static loading in FEM analysis; so the strength of FGM dental implants fabricated by powder metallurgy method under static loading do not reach yield strength and are safe.

7- By comparison of displacement results in experimental works and FEM analysis, it is observed that the maximum displacement value in FGM fixture under static loading in finite element model is much less than displacement values at yield point in experimental tests for FGM implants.

ACKNOWLEDGMENTS

REFERENCES

[1] Mehrali, M., Shirazi, F. S., Mehrali, M., Metselaar, H. S. C., Kadri, N. A. B., and Osman, N. A. A., "Dental implants from functionally graded materials", Journal of Biomedical Materials Research Part A, Vol. 101, No. 10, 2013, pp. 3046-3057.

[2] Chu, C., Zhu, J., Yin, Z., and Wang, S, "Hydroxyapatite–Ti functionally graded biomaterial fabricated by powder metallurgy", Materials Science and Engineering: A, Vol. 271, No. 1, 1999, pp. 95-100.

[3] Shen, H., "Functionally Graded Materials: Nonlinear Analysis of Plates and Shells", Taylor & Francis Group, USA, 2009.

[4] Sadollah, A., Bahreininejad, A., "Optimum gradient material for a functionally graded dental implant using metaheuristic algorithms", Journal of the Mechanical Behavior of Biomedical Materials,. Vol. 4, No. 7, 2011, pp. 1384-1395.

[5] Watari, F., Yokoyama, A., Matsuno, H., Saso, F., Uo, M., and Kawasaki, T., "Biocompatibility of titanium/hydroxyapatite and titanium/cobalt functionally graded implants", Materials science forum,Trans Tech Publ, Vol. 308, 1999, pp. 356-361.

[6] Fujii, T., Tohgo, K., Araki, H., Wakazono, K., Ishikura, M., and Shimamura, Y., "Fabrication and strength evaluation of biocompatible ceramic-metal composite materials", Journal of Solid Mechanics and Materials Engineering, Vol. 4, No. 11, 2010, pp. 1699-1710.

[7] Watari, F., Yokoyama, A., Saso, F., Uo, M., and Kawasaki, T., "Fabrication and properties of functionally graded dental implant", Composites Part B: Engineering, Vol. 28, No.1, 1997, pp. 5-11.

[8] Watari, F., Yokoyama, A., Omori, M., Hirai, T., Kondo, H., Uo, M., and Kawasaki, T., "Biocompatibility of materials and development to functionally graded implant for bio-medical application", Composites Science and Technology, Vol. 64, No. 6, 2004, pp. 893-908.

[9] Watari, F., Yokoyama, A., Saso, F., Uo, M., Matsuno, H., and Kawasaki, T., "Imaging of gradient structure of titanium/apatite functionally graded dental implant", Journal-Japam Insttute of Metals, Vol. 62, 1998, pp. 1095-1101.

[10] Watari, F., Kondo, H., Miyao, R., Omori, M., Okubo, A., Hirai, T., Yokoyama, A., Uo, M., Tamura, Y., and Kawasaki, T., "Effect of spark plasma sintering pressure on the properties of functionally graded implant and its biocompatibility", Journal of the Japan Society of Powder and Powder Metallurgy(Japan), Vol. 49, No. 12, 2002, pp. 1063-1069.

[11] Sasaki, H., Asaoka, T., "The fabrication of Ti alloy-hydroxy apatite(HAp) functionally graded material(FGM)", Journal of the Japan Society of Powder and Powder Metallurgy, Vol. 53, No. 6, 2006, pp. 510-514.

[12] Chu, C., Zhu, J., Yin, Z., and Lin, P., "Structure optimization and properties of hydroxyapatite-Ti symmetrical functionally graded biomaterial", Materials Science and Engineering: A, Vol. 316, No. 1-2, 2001, pp. 205-210.

[13] Chu, C., Zhu, J., Yin, Z., and Lin, P., "Optimal design and fabrication of hydroxyapatite-Ti asymmetrical functionally graded biomaterial", Materials Science and Engineering: A, Vol. 348, No. 1-2, 2003, pp. 244-250.

[14] Bishop, A., Lin, C. Y., Navaratnam, M., Rawlings, R.D., and McShane, H.B., "A functionally gradient material produced by a powder metallurgical process", Journal of materials science letters, Vol. 12, No. 19, 1993, pp. 1516-1518.

[15] Takahashi, H., "Mechanical properties of functional gradient materials of titanium-apatite and titanium zirconia for dental use", Journal of the Japanese Society for Dental Materials and Devices, Vol. 12, No. 5, 1993, pp. 595-612.

[16] Teng, L. D., Wang, F. M., and Li, W. C., "Thermodynamics and microstructure of Ti–ZrO2 metal–ceramic functionally graded materials", Materials Science and Engineering: A, Vol. 293, No. 1-2, 2000, pp. 130-136,.

[17] Lin, K. L., Lin, C. C., "Reaction between titanium and zirconia powders during sintering at 1500 C", Journal of the American Ceramic Society, Vol. 90, No. 7, 2007, pp. 2220-2225.

[18] Takahashi, H., Watari, F., Nishimura, F., and Nakamura, H., "Study of Functionally Gradient Materials of Titanium-apatite and Titanium-silica for Dental Use", Journal of the Japanese Society for Dental Materials and Devices, Vol. 11, No. 3, 1992, pp. 462-468.

[19] Kondo, H., Yokoyama, A., Omori, M., Ohkubo, A., Hirai, T., Watari, F., Uo, M., and Kawasaki, T., "Fabrication of titanium nitride/apatite functionally graded implants by spark plasma sintering", Materials transactions, Vol. 45, No. 11, 2004, pp. 3156-3162.

[20] Tamura, Y., Yokoyama, A., Watari, F., Uo, M., and Kawasaki, T., "Mechanical Properties of Surface

Nitrided Titanium for Abrasion Resistant Implant Materials", Materials Transactions, Vol. 43, No. 12, 2002, pp. 3043-3051.

[21] Matsuno, T., Watanabe, K., Ono, K., and Koishi, M., "Preparation of laminated hydroxyapatite/ zirconia sintered composite with the gradient composition", Journal of materials science letters, Vol. 17, No. 16, 1998, pp. 1349-1351.

[22] Guo, H., Khor, K. A., Boey, Y. C., and Miao, X., "Laminated and functionally graded hydroxyapatite/ yttria stabilized tetragonal zirconia composites fabricated by spark plasma sintering", Biomaterials, Vol. 24, No. 4, 2003, pp. 667-675.

[23] Park, J., Lakes, R. S., "Biomaterials: an introduction", Springer Science & Business Media, 2007.

[24] Fathi, M. H., Hanifi, A., "Nano Bio Ceramics", Arkan Danesh, Isfahan, 2007.

[25] Fathi, M. H., Mortazavi, V., "Medical Application of Bioceramic Coatings for Implants", 2nd ed., Arkan Danesh, Isfahan, 2002.

[26] Hirschhorn, J. S., Reynolds, J. T., and Korstoff, E., "Powder metallurgy fabrication of cobalt alloy surgical implant materials", Research in Dental and Medical Materials, Plenum Press, New York, 1969, pp. 137-150.

[27] Hirschhorn, J. S., McBeath, A. A., and Dustoor, M. R., "Porous titanium surgical implant materials", Journal of Biomedical Materials Research, Vol. 5, No. 6, 1971, pp. 49-67.

[28] Becker, B. S., Bolton, J. D., and Youseffi, M., "Production of Porous Sintered Co–Cr–Mo Alloys for Possible Surgical Implant Applications: Part 1: Compaction, Sintering Behaviour, and Properties", Powder metallurgy, Vol. 38, No. 3, 1995, pp. 201-208.

[29] Becker, B., Bolton, J., "Production of porous sintered Co–Cr–Mo alloys for possible surgical implant applications: part 2: corrosion behaviour", Powder metallurgy, Vol. 38, No. 4, 1995, pp. 305-313.

[30] Becker, B. S., D Bolton, J., "Corrosion behaviour and mechanical properties of functionally gradient materials developed for possible hard-tissue applications", Journal of Materials Science: Materials in Medicine, Vol. 8, No. 12, 1997, pp. 793-797.

[31] Kawasaki, A., Watanabe, R., "Concept and P/M fabrication of functionally gradient materials", Ceramics international, Vol. 23, No. 1, 1997, pp. 73-83.

[32] Torabi, A., "Powder Metallurgy", Amir-Kabir, Isfahan, 1992.

[33] Misch, C. E., "Contemporary implant dentistry", Elsevier Health Sciences, 2007.

[34] Kayabaşı, O., Yüzbasıoğlu, E., and Erzincanlı, F., "Static, dynamic and fatigue behaviors of dental implant using finite element method", Advances in Engineering Software, Vol. 37, No. 10, 2006, pp. 649-658.

[35] Natali, A. N., Pavan, P. G., and Ruggero, A. L., "Analysis of bone–implant interaction phenomena by using a numerical approach", Clinical oral implants research, Vol. 17, No. 1, 2006, pp. 67-74.

[36] Kalanović, M., Zdravković-Petrović, N., Milošević, M., Nikolić, D., Zdravković, N., Filipović, N., and Kojić, M., "Three-dimensional finite element stress analysis of SKY implant system", Journal of the Serbian Society for Computational Mechanics, Vol. 4, No. 2, 2010, pp. 87-96.

[37] Chen, L. J., Hao, H. E., Li, Y. M., Ting, L., Guo, X. P., and Wang, R. F., "Finite element analysis of stress at implant–bone interface of dental implants with different structures", Transactions of Nonferrous Metals Society of China, Vol. 21, No. 7, 2011, pp. 1602-1610.

[38] Lin, C. L., Wang, J. C., and Kuo, Y. C., "Numerical simulation on the biomechanical interactions of tooth/implant-supported system under various occlusal forces with rigid/non-rigid connections", Journal of Biomechanics, Vol. 39, No. 3, 2006, pp. 453-463,.

[39] Meijer, H. J. A., Starmans, F. J. M., Steen, W. H. A., and Bosman, F., "A three-dimensional, finite-element analysis of bone around dental implants in an edentulous human mandible", Archives of Oral Biology, Vol. 38, No. 6, 1993, pp. 491-496.

[40] Williams, K. R., Williams, A. D. C., "Impulse response of a dental implant in bone by numerical analysis", Biomaterials, Vol. 18, No. 10, 1997, pp. 715-719.

[41] Huang, H. M., Lee, S. Y., Yeh, C. Y., and Lin, C. T., "Resonance frequency assessment of dental implant stability with various bone qualities: a numerical approach", Clinical Oral Implants Research, Vol. 13, No. 1, 2002, pp. 65-74.

[42] Hedia, H. S., Mahmoud, N. A., "Design optimization of functionally graded dental implant, Bio-Medical Materials and Engineering", Vol. 14, No. 2, 2004, pp. 133-143.

[43] Hedia, H. S., "Design of functionally graded dental implant in the presence of cancellous bone", Journal of Biomedical Materials Research Part B: Applied Biomaterials, Vol. 75, No. 1, 2005, pp. 74-80.

[44] Yang, J., Xiang, H. J., "A three-dimensional finite element study on the biomechanical behavior of an FGBM dental implant in surrounding bone", Journal of Biomechanics, Vol. 40, No. 11, 2007, pp. 2377-2385.

[45] Lin, D., Li, Q., Li, W., and Swain, M., "Bone remodeling induced by dental implants of functionally graded materials", Journal of Biomedical Materials Research Part B: Applied Biomaterials, Vol. 92, No. 2, 2010, pp. 430-438.

[46] Lin, D., Li, Q., Li, W., Zhou, S., and Swain, M.V., "Design optimization of functionally graded dental implant for bone remodeling", Composites Part B: Engineering, Vol. 40, No. 7, 2009, pp. 668-675.

[47] Koudarian, R., Hafez-Quran, A., "Finite element analysis in dental implants", Shayan Nemoudar, Tehran, 2012.

[48] Fathi, M. H., Mortazavi, V., "Properties and applications of metallic biomaterials", Arkan, Isfahan, 2003.

[49] Khodaei, M., Meratian, M., and Savabi, O., "Effect of spacer type and cold compaction pressure on structural and mechanical properties of porous titanium scaffold", Powder Metallurgy, Vol. 58, No. 2, 2015, pp. 152-160.

[50] Ivanoff, C. J., Grondahl, K., Sennerby, L., Bergstrom, C., and Lekholm, U., "Influence of variations in implant diameters: a 3-to 5-year retrospective clinical report ," International Journal of Oral and Maxillofacial Implants, Vol. 14, No. 2, 1999, pp. 173-180.

[51] Steigenga, J. T., Al-Shammari, K. F., Nociti, F. H., Misch, C. E., and Wang, H. L., "Dental implant design and its relationship to long-term implant success", Implant dentistry, Vol. 12, No. 4, 2003, pp. 306-317.

[52] Kong, L., Liu, B., Li, D., Song, Y., Zhang, A., Dang, F., Qin, X., and Yang, J., "Comparative study of 12 thread shapes of dental implant designs: a three-dimensional finite element analysis", World Journal of Modelling and Simulation, Vol. 2, No. 2, 2006, pp. 134-140.

[53] Rho, J. Y., Ashman, R. B., and Turner, C. H., "Young's modulus of trabecular and cortical bone material: Ultrasonic and microtensile measurements", Journal of Biomechanics, Vol. 26, No. 2, 1993, pp. 111-119.

[54] Benzing, U. R., Gall, H., and Weber, H., "Biomechanical aspects of two different implant-prosthetic concepts for edentulous maxillae", International Journal of Oral & Maxillofacial Implants, Vol. 10, No. 2, 1995, pp. 188-198.

[55] ANSYS, Multiphysics, Software Help, Ver. 14.0, United States, 2011.

[56] Mericske-stern, R., Piotti, M., and Sirtes, G., "3-D in vivo force measurements on mandibular implants supporting overdentures. A comparative study", Clinical oral implants research, Vol. 7, No. 4, 1996, pp. 387-396.

[57] Chun, H. J., Cheong, S. Y., Han, J. H., Heo, S. J., Chung, J. P., Rhyu, I. C., Choi, Y. C., Baik, H. K., Ku, Y., and Kim, M. H., "Evaluation of design parameters of osseointegrated dental implants using finite element analysis", Journal of oral rehabilitation, Vol. 29, No. 6, 2002, pp. 565-574.